SAND99-0552J

Transient model for keyhole during laser welding.

Vladimir V. Semak*, William David Bragg, Brian Damkroger***, and Steven Kempka*****

* Applied Research Laboratory, Pennsylvania State University, State College, PA 16804
e-mail: vxs21@psu.edu

** Physics Department, New Mexico State University, Las Cruces, NM

*** Sandia National Laboratory, Albuquerque, NM

Abstract

A novel approach to simulating the dominant dynamic processes present during concentrated energy beam welding of metals is presented. A model for transient behavior of the front keyhole wall is developed. It is assumed that keyhole propagation is dominated by evaporation recoil driven melt expulsion from the beam interaction zone. Results from the model show keyhole instabilities consistent with experimental observations of metal welding, metal cutting and ice welding.

Evaporation from a surface irradiated with a laser beam is an important process affecting energy transfer, melt hydrodynamics, and chemical composition of the processed work piece. A model of laser induced evaporation for surface temperatures below critical was developed by Anisimov [1]. In particular, this model provides the value of evaporation recoil pressure, which is the dominant factor determining melt motion [2] at elevated surface temperatures.

Although high surface temperature and high recoil pressure can be achieved in keyhole laser welding, Anisimov's model has not been applied in welding simulation except for a few notable recent attempts [3,4]. Previous models of laser and e-beam welding considered a steady state keyhole and disregarded the effects of melt motion, related convective heat transfer, and hydrodynamic instabilities. These over-simplified, unphysical assumptions produced models valid only for conduction limited welding and lacking the accuracy required for industrial application.

A transient model of laser welding incorporating evaporation recoil pressure was recently suggested by Semak [5]. The proposed concept is based on a set of experimentally verified [6-12] assumptions: (1) the front part of the keyhole wall is directly exposed to the laser beam; (2) the propagation of the front keyhole wall is due to drilling-like melt expulsion, generated by the evaporation recoil pressure; and (3) the back of the keyhole stays mostly outside the laser beam. This physical scheme was additionally confirmed by the results of high-speed photography of ice welding with a low power CO2 laser (Fig.1).

Using the new physical scheme, the keyhole laser welding model can be divided into three major interdependent parts: the front part of the keyhole, the back and side walls of the keyhole, and the bulk of the weld pool. Here the dynamics of the front wall

DISCLAIMER

of the keyhole were simulated. The melt layer was modeled as a thin boundary layer of width similar to the beam diameter (Fig.2). For the calculations we assumed surface absorption of laser power (no volumetric heat generation) [13], temperature independent material properties, and 1D melt flow driven dominantly along the highest gradient of recoil pressure (x-axis, Fig.2). Under these conditions, the melt flow can be adequately modeled by St. Venant's equations for incompressible, open-channel flow modified to include mass source and sink due to melting and evaporation, respectively:

$$\frac{\partial h}{\partial t}+\frac{\partial (v_x h)}{\partial x}=-V_{dv}+V_m, \tag{1}$$

$$\frac{\partial (v_x h)}{\partial t}+\frac{\partial}{\partial x}\overline{hv_x^2}+\frac{ph}{\rho}\sqrt{=}\frac{p}{\rho}\frac{\partial h}{\partial x}-(V_{dv}-V_m)v_x-\frac{\mu}{\rho}\frac{v_x}{h}. \tag{2}$$

The x direction is along the melt surface (Fig.2), the z direction is a local normal to the melt surface, h is the melt thickness, v_x is the melt flow velocity averaged over the melt layer thickness, ρ is the density of the condensed phase, p is the pressure across the molten layer, μ is melt viscosity, V_{dv} is the component of vapor-liquid boundary velocity due to evaporation, and V_m is the melt front velocity.

A mixed-type boundary condition is applied on the liquid - vapor boundary

$$-k\left.\frac{\partial T}{\partial z}\right|_{surf}+\rho V_{dv}L_v=(1-R)I_{laser}, \tag{3}$$

where k is the heat conductivity of solid or liquid phase, $\left.\frac{\partial T}{\partial z}\right|_{surf}$ is the temperature gradient at the surface, R is the reflection coefficient for the laser wavelength, and I_{laser} is the intensity of the laser beam at the surface. For typical welding conditions the melt surface temperature is much lower than the critical temperature and the energy of evaporation of a single atom, U, can be approximated as a constant. Then the evaporation velocity, V_{dv}, can be expressed by the equation [1]

$$V_{dv}=V_0\exp(-U/kT_{surf}), \tag{4}$$

where V_0 is a coefficient of the order of magnitude of velocity of sound, and T_{surf} is the local surface temperature. Note that this boundary condition (3,4) differs from the commonly used "Problem of Stefan" boundary condition. The surface temperature is not fixed at the boiling point and depends on absorbed intensity.

In welding, the melt front propagation velocity is typically small. So, the classical problem of Stefan boundary condition can be applied to the solid-liquid boundary (melting front $z = Z_m$)

$$\rho L_m V_m=k_s\left.\frac{\partial T_s}{\partial z}\right|_{z=Z_m}-k_l\left.\frac{\partial T_l}{\partial z}\right|_{z=Z_m}, \tag{5}$$

where L_m is the latent heat of melting, subscripts "s" and "l" are for solid and liquid, respectively.

The velocity of the melt surface, V_d, is given by the following equation:

$$V_d = -\frac{f(v_x h)}{fx} - V_{dv}. \qquad (6)$$

Because the boundary layer is assumed thin, the pressure across the molten layer, p, is approximated by the evaporation recoil pressure applied to the melt surface, p_r. The surface temperature and the evaporation recoil pressure are related according to the equation

$$p_r = AB_0 T_{surf}^{-1/2} \exp(-U/kT_{surf}), \qquad (7)$$

where A is a coefficient dependent on ambient pressure, and B_0 is an empirical constant [1]. The pressure of the vapor inside keyhole is the "ambient" pressure and is dependent on keyhole geometry. The coefficient A provides the front keyhole model "feedback" dependence on other weld pool parameters.

Taking into consideration motion of the melt and heat source (surface of the keyhole), the heat transfer equations for the liquid and solid phases can be presented in the following form:

$$\frac{fT}{ft} + v_x \frac{fT}{fx} + V_d \frac{fT}{fz} = \frac{k_l}{\rho_l c_l}\left(\frac{f^2T}{fx^2} + \frac{f^2T}{fy^2} + \frac{f^2T}{fz^2}\right), \qquad (8)$$

$$\frac{fT}{ft} + V_d \frac{fT}{fz} = \frac{k_s}{\rho_s c_s}\left(\frac{f^2T}{fx^2} + \frac{f^2T}{fy^2} + \frac{f^2T}{fz^2}\right). \qquad (9)$$

Here "l" and "s" refer to the liquid and solid phases and ρ, c, T, and k are the density, specific heat, temperature and heat conductivity, respectively.

The system of differential equations (1,2,8,9) with the boundary conditions (3,5) and equations (4,6,7) represent the mathematical formulation of the transient physical model of the front keyhole wall. Solution of these equations provides temporal evolution of the front keyhole shape, melt temperature, and the velocity of melt ejection from interaction zone. Laser cutting can also be modeled with this approach because the propagation of the cutting front is similarly due to evaporation recoil driven melt expulsion from the beam interaction zone.

The simulation results confirm the development of a step-like shape of the front part of the keyhole (Fig.3) predicted earlier using a semi-empirical model [3]. This instability of the keyhole occurs when the component of the keyhole velocity, V_d, along the sample surface (axis y^*, Fig.2) exceeds beam translation speed. Then front wall of the keyhole "runs" away from the laser beam and this produces humps on the keyhole wall. The humps originate at the top and move down the keyhole wall. Consequently, related melt ejection and evaporation from the front of keyhole vary in space in time affecting quality of both welding and cutting [6]. In the area of a hump, high velocity melt flow is generated resulting in additional melting of material from the sides of the cut. The observed striations on the edge of laser cuts correspond to the trajectories of individual humps. The model predicts that the humping of the welding or cutting front does not occur if the y^* component of the velocity V_d is smaller than the beam translation speed. This particular result demonstrates the significant practical value of the new model in predicting dynamic phenomena.

The calculations show that the size of the hump along the axis y^* is approximately 20 – 50 μm. The surface temperature and, consequently, recoil pressure are higher in the area of the hump. Therefore, the recoil pressure gradient along the keyhole wall (y-axis) can exceed that across the wall (x-axis). This can generate a large component of flow velocity along the keyhole wall due to melt acceleration as the hump moves down the keyhole wall. The existence of such "downward" flow is confirmed by x-ray photography of metal welding [6] and our ice welding experiments. This indicates that our assumption, that the recoil pressure gradient across the wall is dominant and that the flow is 1D along the x-axis, is a rough approximation. In future calculations this assumption will be improved and 2D melt flow will be simulated.

Acknowledgment

This work was performed at Pennsylvania State University and New Mexico State University with financial support from Sandia National Laboratory. Sandia is a multiprogram laboratory operated by Sandia Corporation, a Lockheed Martin Company, for the United States Department of Energy under Contract DE-AC04-94AL85000.

References

1. S.I.Anisimov and V.A.Khokhlov, *Instabilities in Laser - Matter Interaction*, 1995 (CRC Press, Boca Raton, FL).
2. M. von Almen, Laser drilling velocity in metals, (1976) *J. Appl. Phys.*, v.47(12), pp.5460-5463.
3. A. Matsunawa and V. Semak, Simulation of the Front Keyhole Wall Dynamics During Laser Welding. *Journal of Physics D: Applied Physics* (1997) 30, p.798.
4. V. Semak and A. Matsunawa Role of the Recoil Pressure in Energy Balance During Laser Welding. *Journal of Physics D: Applied Physics* (1997) 30, p.2541.
5. V. Semak, J. A. Hopkins, M. H. McCay, and T. D. McCay A Concept for a Hydrodynamic Model of Keyhole Formation During Laser Welding, *Proc. ICALEO'94*, 1994 pp.641-650.
6. Y. Arata. Plasma, *Electron and Laser Beam Technology. Development and Use in Material Processing* p.392,424,1986 (American Society for Metals: Metal Park, OH).
7. V. Semak, J. A. Hopkins, M., H. McCay and T. D. McCay, Measurement of Melt Pool Dynamics During Laser Welding *J. Phys.D: Applied Physics,* 1995 (1995) 28, pp.2443-2450
8. A. Matsunawa, J.-D. Kim, S. Katayama, and V. Semak Experimental Study and Numerical Modeling of Melt Hydrodynamics During CO2 Laser Welding, *Proc. ICALEO'96*, 1996
9. V. Semak, J. C. West, J. A. Hopkins, M. H. McCay, and T. D. McCay, Shape and Position of Keyhole During Laser Welding, *Proc. Of ICALEO'95*, 1995, pp.544-552.
10. V. Semak, M. H. McCay, and T. D. McCay Comparison of IR and UV Emittance Distributiona Along the Surface During CO2 Laser Welding, *Proc.ICALEO'93*, pp.777-782.

11. V. Semak, J. A. Hopkins, M. H. McCay, and T. D. McCay Dynamics of Penetration Depth During Laser Welding *Proc. ICALEO'94*, 1994, pp.830-837.
12. R. Fabbro and A. Poueyo-Verwaerde, Modeling of Deep Penetration Laser Welding Process: Application to the Analysis of the Energy Coupling, *Proc. ICALEO'95*, 1995, pp.979-988.
13. Yu. V. Afanasiev and O. N. Krokhin, Sov. Phys. JETP, 1967, v.25, p. 639.

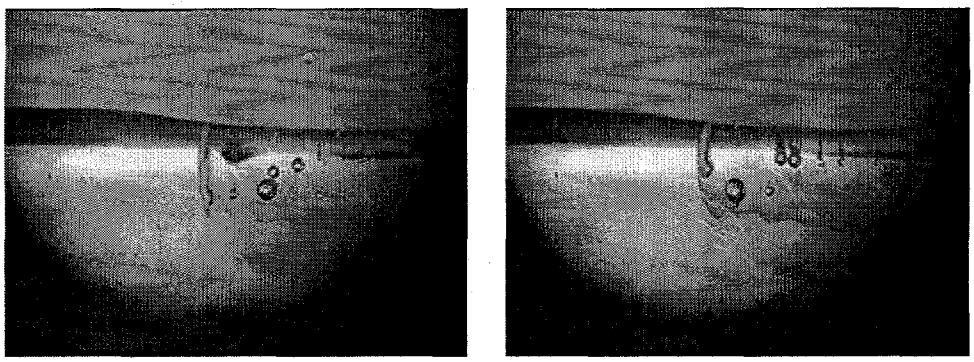

Figure 1. Frame sequence from high speed photography of ice welding using a CO_2 laser [33]. Laser power is 70 W, beam translation speed is 2 cm/s. The frame exposure is 1/4000 s, and the interval between the frames is 330 ms.

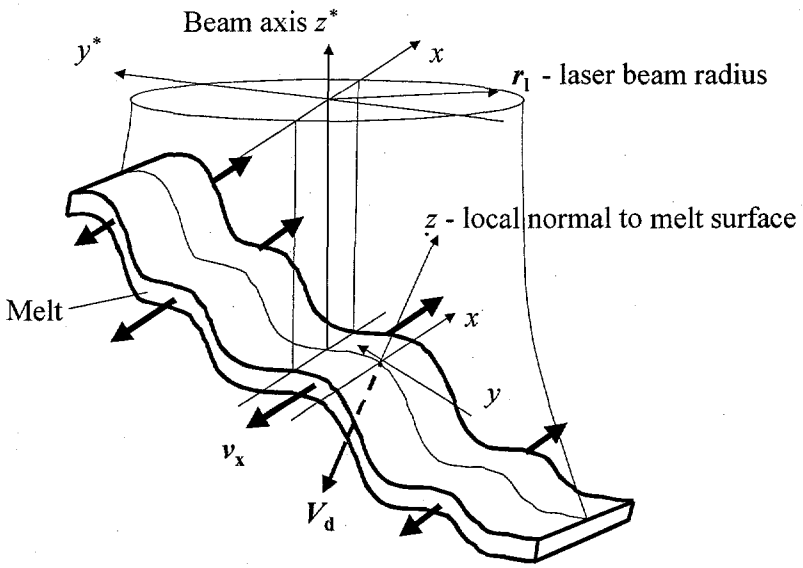

Figure 2. Schematic of the front keyhole wall. Local coordinate system x, y, z is such that z-axis is directed along the local normal to the melt surface.

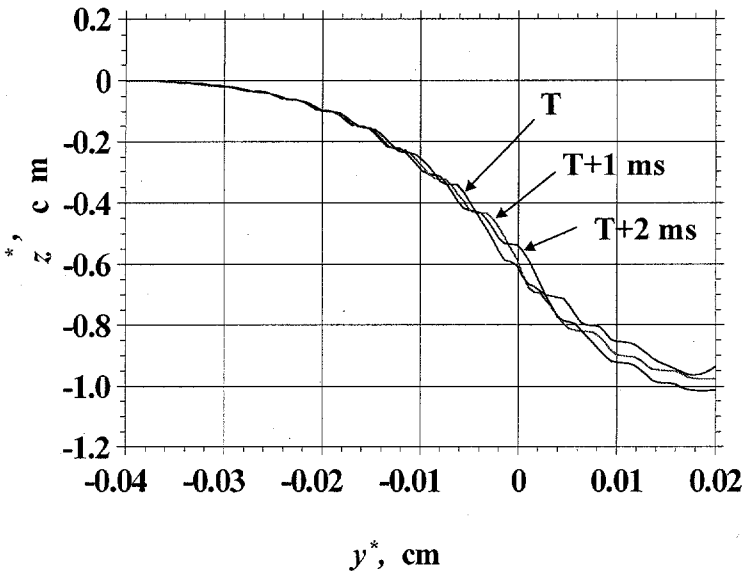

Figure 3. Temporal evolution of the front part of keyhole for the following processing parameters: Gaussian beam intensity distribution with maximum of 3 MW/cm^2 and radius 200μm, beam translation speed of 20 mm/s.